**Forschungszentrum Karlsruhe**
in der Helmholtz-Gemeinschaft

**Wissenschaftliche Berichte**
FZKA 7052

# 3-Balls-on-3-Balls Test for Ceramic Disks: A Finite Element Study

**T. Fett, G. Rizzi**

**Institut für Materialforschung**

**November 2004**

**FORSCHUNGSZENTRUM KARLSRUHE**

in der Helmholtz-Gemeinschaft

Wissenschaftliche Berichte

**FZKA 7052**

# 3-BALLS-ON-3-BALLS TEST FOR CERAMIC DISKS:

# A FINITE ELEMENT STUDY

**T. Fett, G. Rizzi**

Institut für Materialforschung

Forschungszentrum Karlsruhe GmbH, Karlsruhe

2004

**Impressum der Print-Ausgabe:**

**Als Manuskript gedruckt**


**Forschungszentrum Karlsruhe GmbH**
**Postfach 3640, 76021 Karlsruhe**

**Mitglied der Hermann von Helmholtz-Gemeinschaft**
**Deutscher Forschungszentren (HGF)**

**ISSN 0947-8620**

**urn:nbn:de:0005-070521**

## 3-balls-on-3-balls test for ceramic disks: A finite element study

Abstract:
In the usual tests to determine strength or lifetime under tension, bending or compression loading, a uniaxial stress state is present. However, in components very often multiaxial stresses occur. But also under uniaxial external loading, multiaxial stresses are possible, for instance, in notched components. Common tests are bending tests on thin circular disks.
Following the description of conventional tests, a recently developed test using 3 loading and 3 supporting balls shall be addressed. For this test, the maximum principal stresses and the biaxiality are determined for a wide range of geometries by using the finite element method.

## Eine Vorrichtung zur Bestimmung der Festigkeit von keramischen Scheibenproben: Finite Elemente-Berechnungen

Kurzfassung:
Bei der mechanischen Festigkeitscharakterisierung von keramischen Werkstoffen im Zug-, Biege- und Druckversuch wird das Versagen unter einachsiger Belastung geprüft. In realen Bauteilen treten jedoch meist mehrachsige Spannungszustände auf. Deshalb wurden schon früh experimentelle Methoden entwickelt, um das Festigkeitsverhalten unter mehrachsigen Spannungszuständen in kreisförmigen Scheiben zu bestimmen. Nach einer Beschreibung der bisherigen Methoden wird auf ein neues Verfahren mit drei Belastungs- und drei Unterstützungskugeln eingegangen. Durch Finite Elemente-Rechnungen werden die maximalen Hauptspannungen und die Mehrachsigkeit in diesem Versuch berechnet.

# Contents

## 1. Introduction

Conventional strength tests describe the failure behaviour of materials under simple stress conditions, in most cases, uniaxial stresses. In practical applications, however, mechanical loading often leads to multiaxial stresses.
But also under uniaxial external, loading multiaxial stresses are possible, for instance, in notched components. Rotating structures and components under internal pressure exhibit multiaxial stresses. Also thermal stresses generally are multiaxial and on surfaces mostly equibiaxial.
Mechanical strength characterisation of ceramic materials (for an overview see [1]) is mostly carried out by uniaxial tests, e.g.

- Tensile tests [2,3]
- Compression tests on cylindrical specimens [4]
- Compression tests on hollow cylinders [5,6]
- Bending tests [7-9]
- Circular ring test [10,11]
- C-ring test [12,13]

In real components, however, usually multiaxial stress states appear. Therefore, experimental methods were developed quite early to determine the strength and deformation behaviour under multiaxial stress conditions:

- Ring-on-ring test (with its modifications) [14-18]
- Sphere-on-ring test [19-21]
- Ball-on-3-balls test [22-24]
- Brazilian disk test [25-33]
- Thermal shock test [34,35]
- Pressurised tube test [36-39]
- Torsion test

Most of these strength tests require high-quality specimen surfaces (except for the ball-on-3-balls and the thermal shock tests). It is the aim of this report to analyse a simple multiaxial strength test that allows testing of specimens in the "as fired" state. First, the ring-on-ring test with modifications shall be illustrated in detail. Then, a new test with 6 balls shall be addressed [40]. The main part of the report shall then deal with the determination of stresses for a wide range of geometries.

## 2. Biaxial bending tests on disks

### 2.1 Ring-on-ring test

The principle procedure in using the concentric ring-on-ring test is illustrated in Fig. 1 (see e.g. [14]-[18]). A disc-shaped specimen is supported by a ring and loaded by a concentric ring of smaller diameter.

The ring-on-ring test has been extensively used for strength measurements on glass and has been standardized. Whilst bending bars exhibit additional flaws at the edges, generated by the machining process, the edges of a circular disc are nearly free of stress and will not contribute to failure.

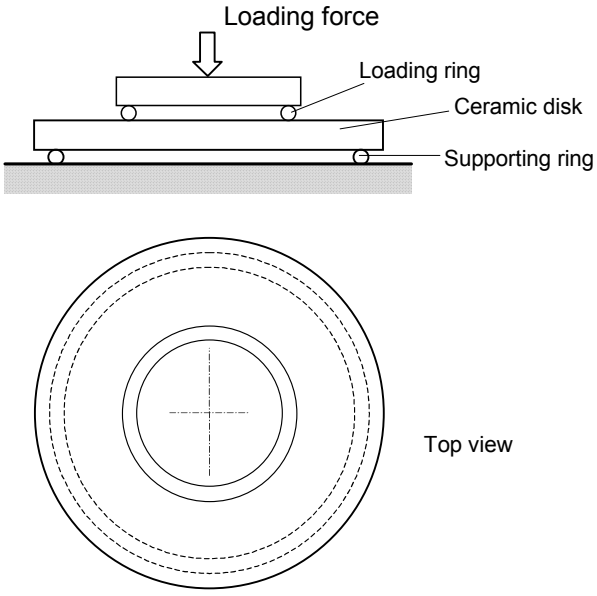


**Fig. 1** Ring-on-ring test

This test device provides for a well-defined stress state only under ideal loading conditions. For this, however, highly plane-parallel disk-shaped specimens are required. If this is not the case, a 3-point contact between ring and specimen will occur at the beginning of the test. Only at high loads will a continuous contact line develop, resulting in the correct stress distribution.

### 2.2 Ring-on-bearing ring test

In a modification of the ring-on-ring test, the supporting ring is replaced by a ball bearing ring (Fig. 2). This ensures reduced friction and simplified supporting conditions. Stress concentrations due to the Hertzian contacts are not of high importance, because the stresses superimposed by bending moments disappear in the supporting region.

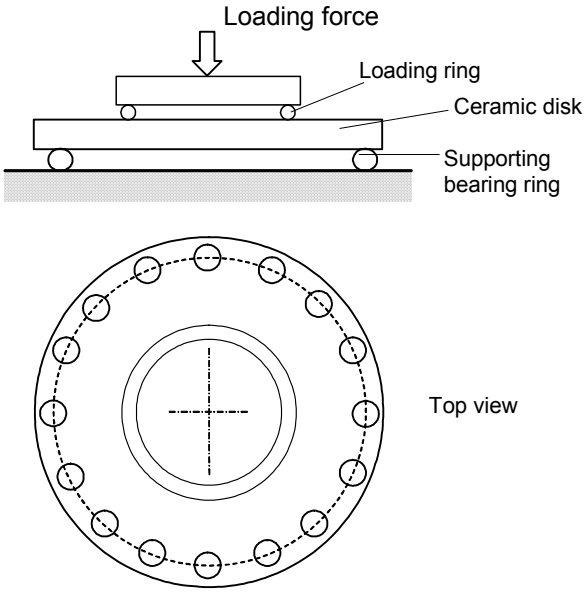


**Fig. 2** Ring-on-bearing ring test

### 2.3 Ball-on-ring test

In order to avoid undefined supporting conditions, the ball-on-ring test was developed. In this test, a disk specimen is supported by a ring and loaded centrally with a ball (see Fig. 3). This test configuration was proposed by Shetty et al. [19][20]. To reduce friction effects between disk and supporting ring, the latter is sometimes replaced by a ball bearing ring (Fig. 4) as used in Section 2.2.

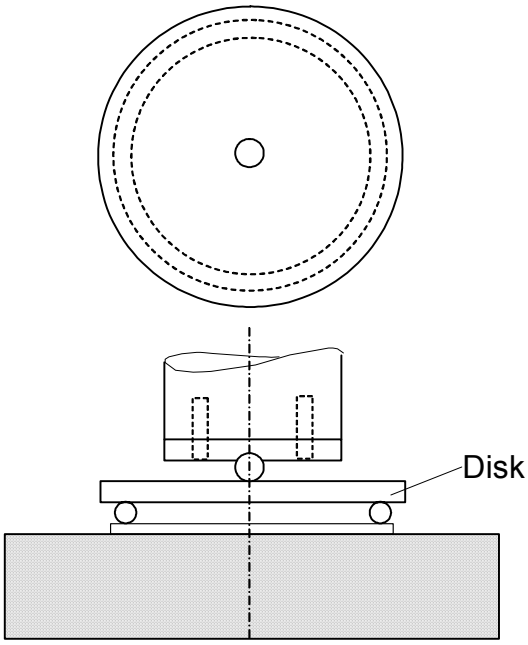


**Fig. 3** Ball-on- ring test

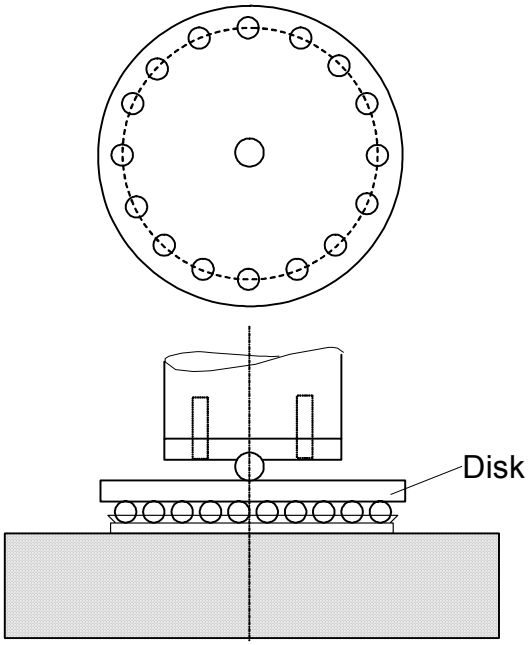


**Fig. 4** Ball-on-bearing ring test

### 2.4 Ball-on-3-balls test

Another modification is the ball-on-3-balls configuration. Here, the outer ring is also replaced by 3 balls. This results in statically well-defined conditions. This test is described in [22]. Extensive computations of stress state are given in [23]. Errors resulting from misalignments and test specimen imperfections are discussed in [24].

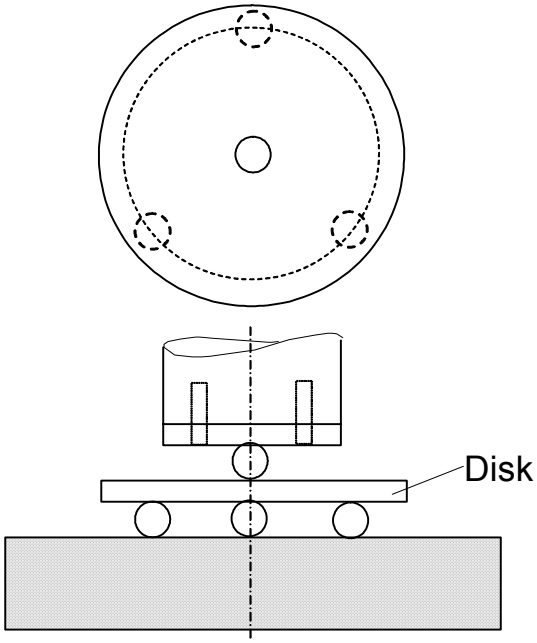


**Fig. 5** Ball-on-3-balls test

## 3. A new 3-balls-on-3-balls test

As already mentioned before, the ball-on-3-balls test yields statically well-defined mechanical boundary conditions. A disadvantage of this test configuration, however, is the relatively small effective surface tested. Due to the strongly decreasing stresses with increasing distance from the disk centre, the plate regions at larger distance hardly contribute to the failure behaviour.

This was the main reason why the test was modified [40] by reducing the influence of the point-like stress spots and significantly increasing the effective surface tested. As shown in Fig. 6, the outer supporting and the inner loading forces are applied by 3 spheres each. By this configuration, mechanically well-defined supporting conditions as well as well-defined loading conditions are achieved.

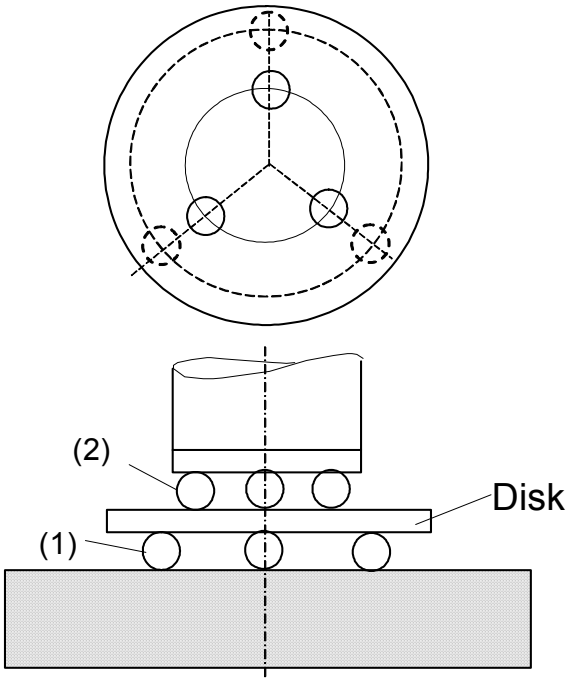


**Fig. 6** 3-balls-on-3-balls test: Loading and supporting spheres in line.

In Fig. 6, the loading and supporting spheres are „in line“, i.e. the sphere centres are located at the same polar angle. Figure 7 shows the case of the inner and outer spheres being shifted by an angle of 60°.

Figure 8 gives a possible design. The loading (1) and supporting balls (2) can move in radial grooves (3) in the two metal plates (4,5) with a small clearance in width direction. For the outer support rolls to move freely to outside during loading, they are pushed to the inner edge by soft springs (6) before the test. On the other hand, the inner loading spheres can move freely from the outer edge to the inside. Besides the spring solution represented in Fig. 8, also a magnet solution may be applied, as it is often done in bend tests. For this, the balls must be made of a magnetisable material (e.g. magnetisable steel).

The exact orientation of the two metal plates (4,5) relative to each other and, hence, the exact location of the supporting and loading balls relative to each other is ensured by two metal pins (7) in the bore holes (8). These pins can be removed before load application in a testing machine.

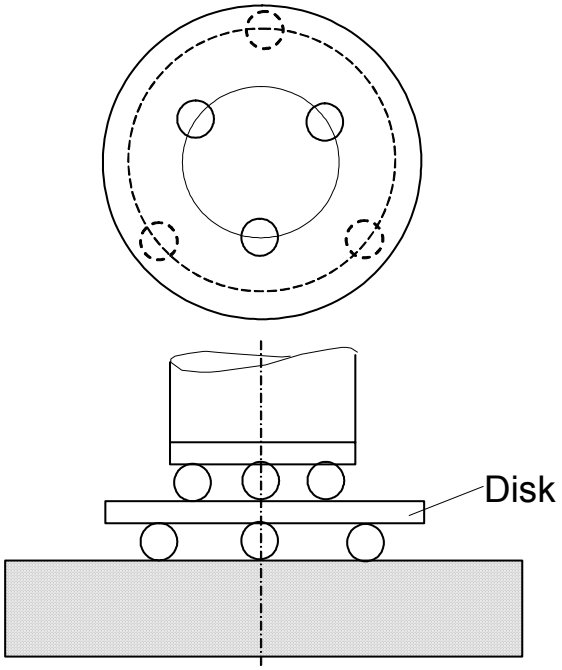


**Fig. 7** 3-balls-on-3-balls test: Loading and supporting spheres in line under an angle of 60°.

Figure 9 illustrates simplified versions of the 3-balls-on-3-balls test (9a) and the ball-on-3-balls test (9b). Two screws (only one shown in Fig. 9a) ensure centric positioning of the disk, resulting in a constant overhang along its circumference.

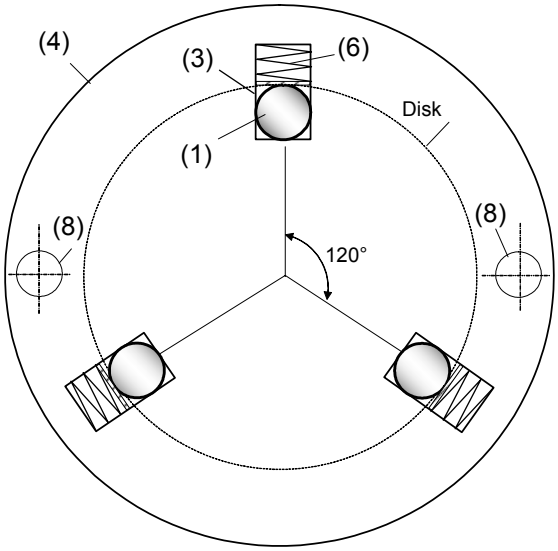

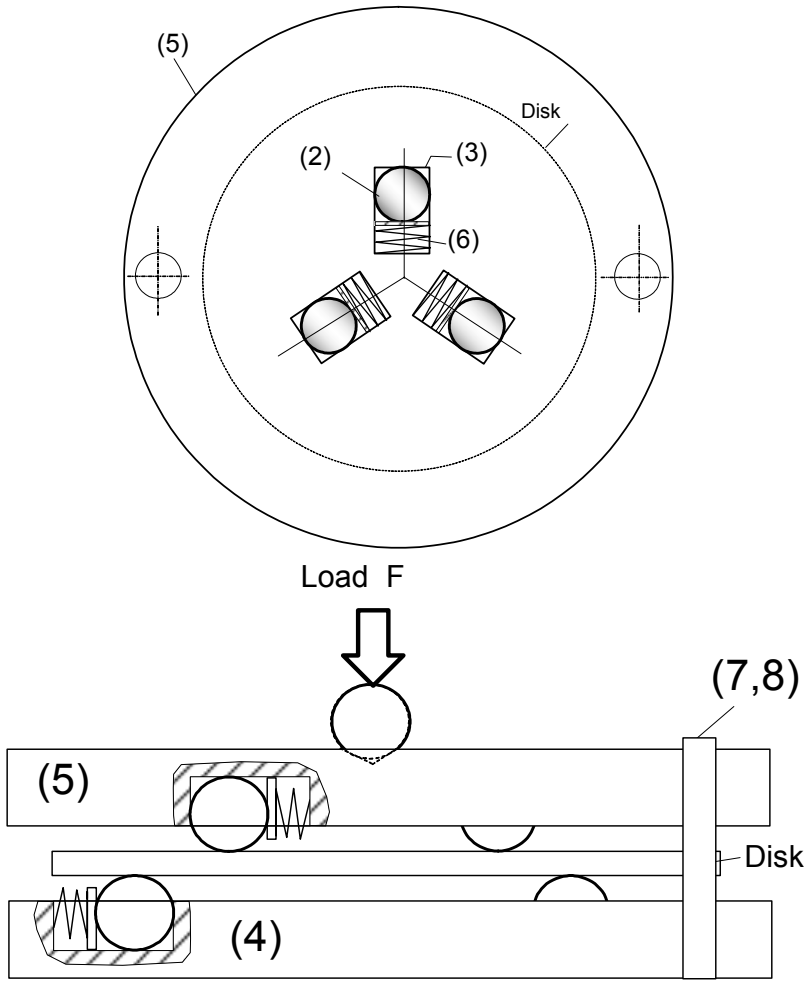


**Fig. 8** A possible design for the test, including all degrees of freedom (free movement of the balls).

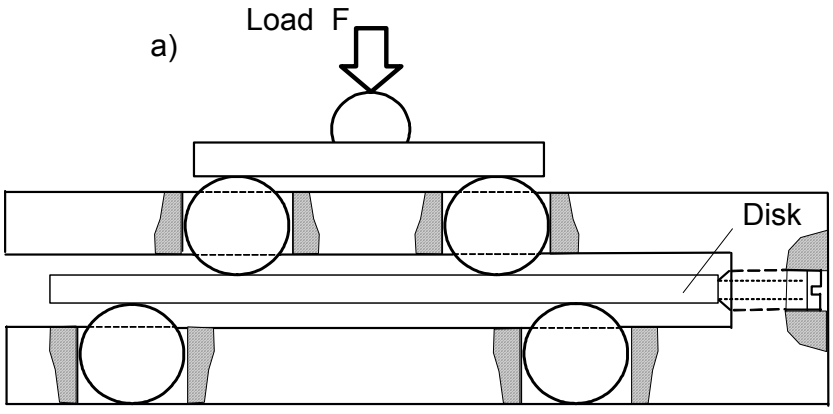

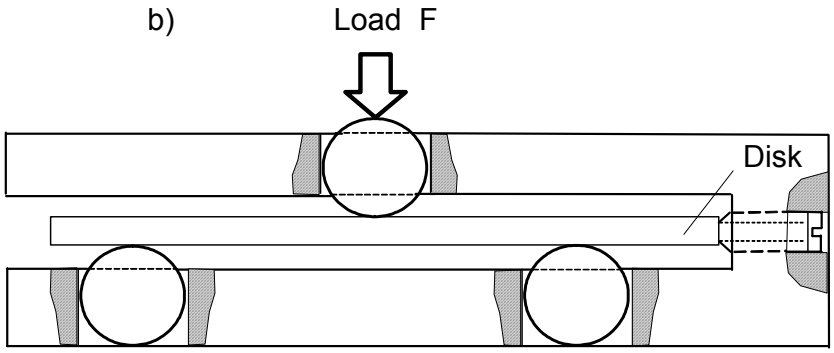


**Fig. 9** Simplified test arrangements for the 3-balls-on-3-balls test (a) and the ball-on-3-balls test (b).

## 4. Finite element computations

Figure 10 shows the disk of radius $R$ and the sphere location circles $R_1$ (loading spheres) and $R_2$ (supporting spheres). The ratio of outer to inner sphere circles was chosen to be $R_1/R_2=2$.

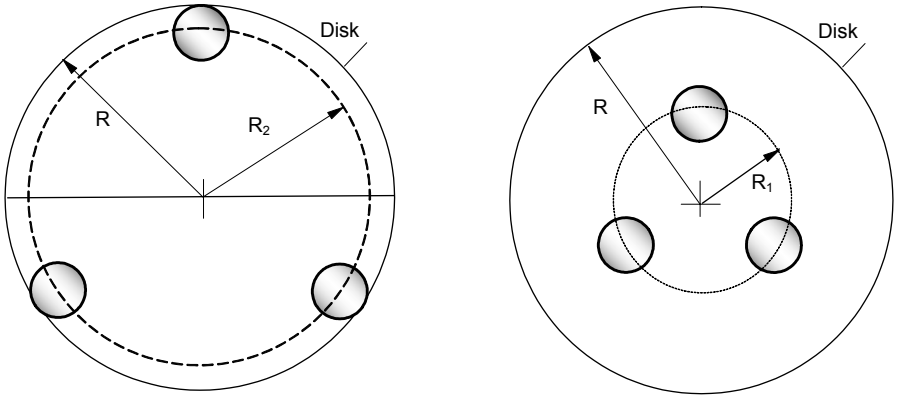


**Fig. 10** Definition of the relevant radii $R$, $R_1$, and $R_2$.

The finite element net is presented in Fig. 11. It may be used for considering the in line sphere application as well as 60° rotation of the inner spheres. In addition, the case of a "ball on 3 balls" can be modelled. The disk was realised by a finite element net of about 24100 elements with 110400 nodes. The computations were carried out with ABAQUS version 6.3. For all FE computations, the radius of the circle on which the inner spheres are located was chosen arbitrarily as $R_1=1$.

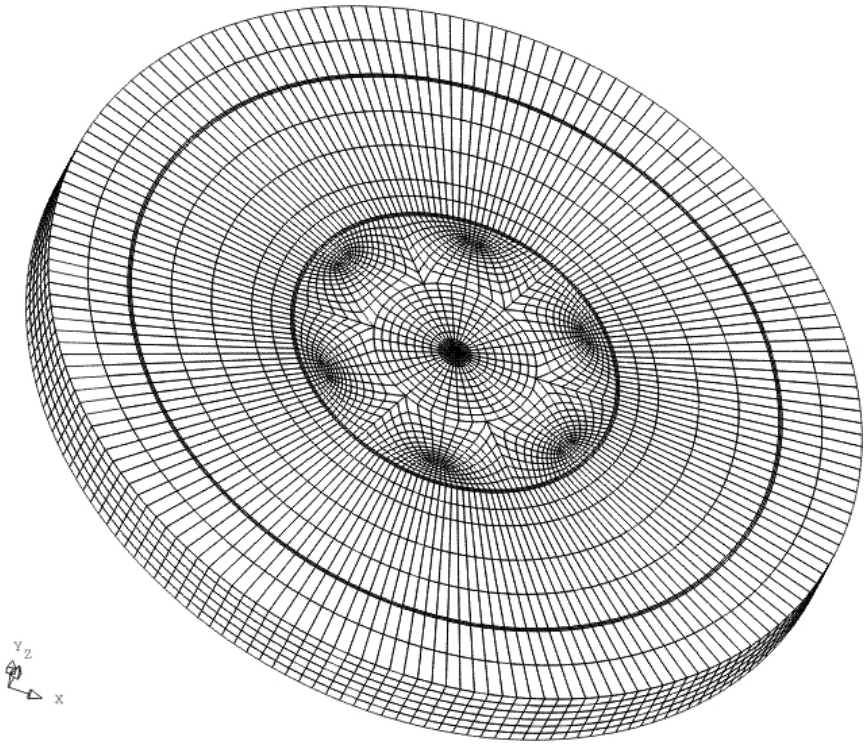

**Fig. 11** Finite element net.

## 4.1 Loading and supporting balls in line

### 4.1.1 Contour plots for the maximum principal stress

The maximum principal stress is represented in Figs. 12 and 13 for the thicknesses $t/R_1$=0.1 and 0.4 and ν=0.25. The stress levels are scaled according to $\sigma_1 t^2/F$.

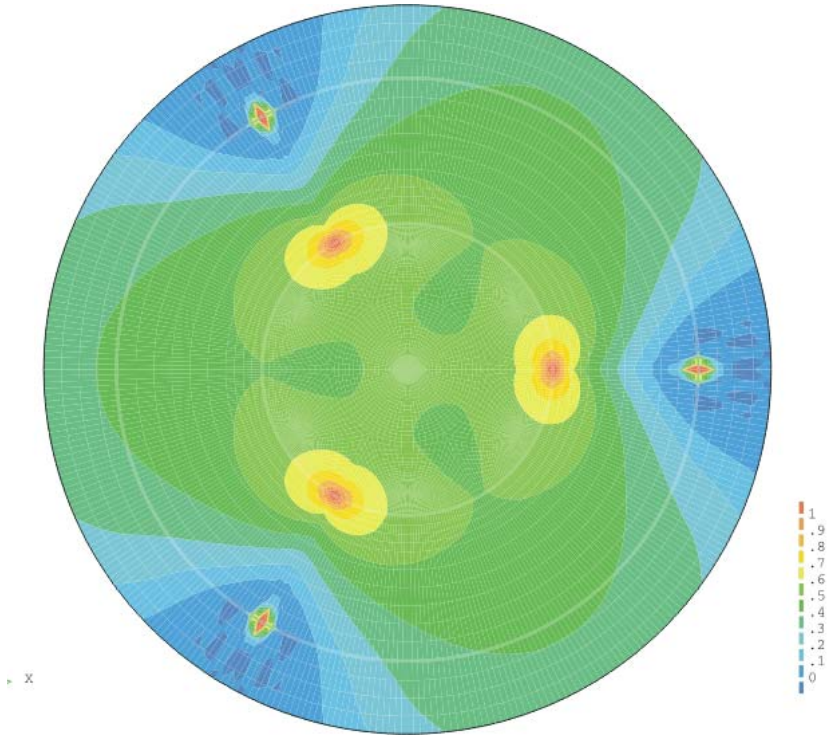


**Fig. 12** Maximum principal stress for $t/R_1$=0.1 and ν=0.25 (blue $\sigma_1 t^2/F$=0, green =0.5, red=1).

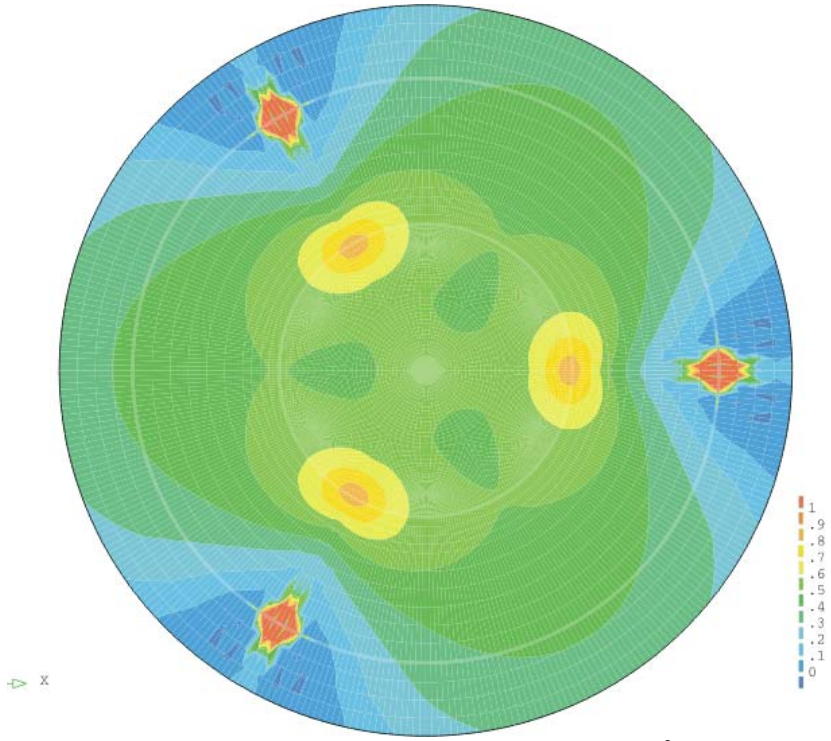


**Fig. 13** Maximum principal stress for $t/R_1$=0.4 and ν=0.25 (blue $\sigma_1 t^2/F$=0, green =0.5, red=1).

Figures 14 and 15 show the ratio of the second (not disappearing) principal stress to the maximum principal stress. It clearly indicates the biaxial stress state with a small variation in the central zone of the disk only. The value "1" represents an equibiaxial stress state. In this context, it should be noted that one of the principal stresses must disappear at the (free) disk surface.

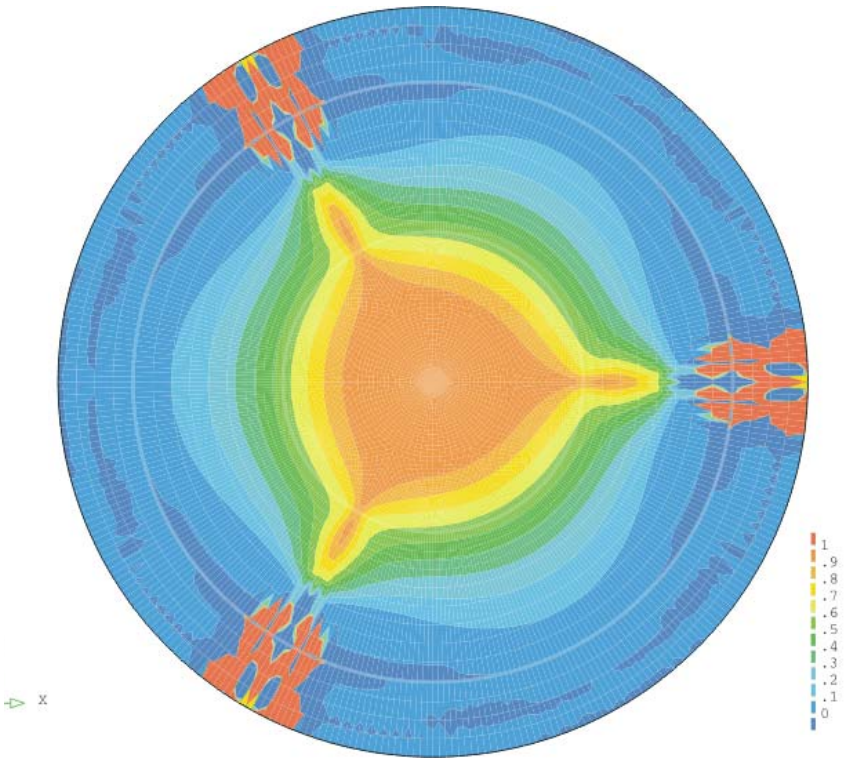


**Fig. 14** Stress biaxiality at the surface for $t/R_1$=0.1 and ν=0.25 (blue $\sigma_2/\sigma_1$=0, green=0.5, red=1).

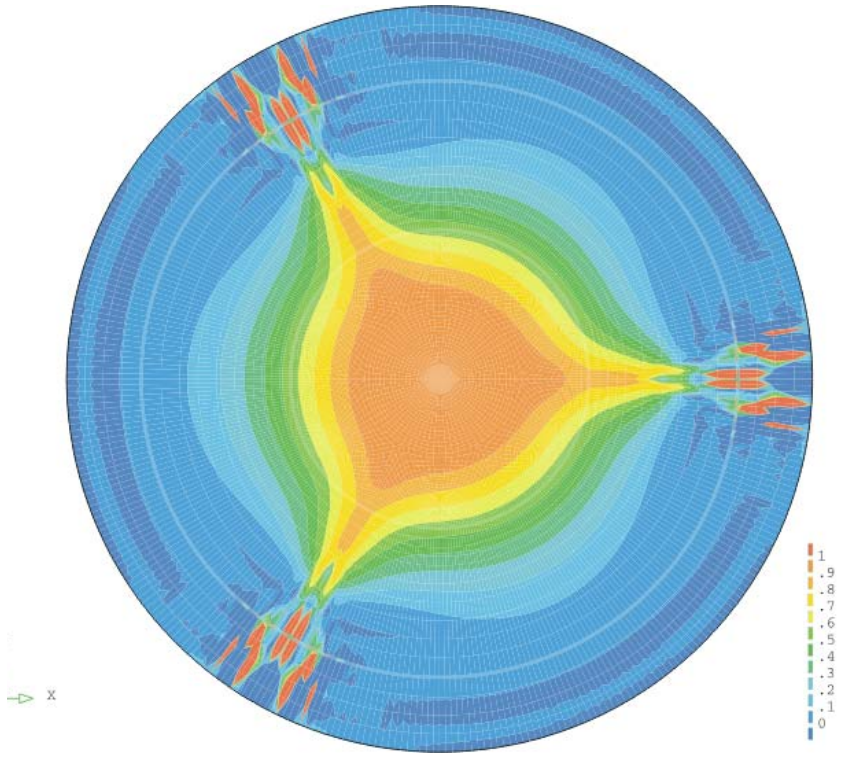


**Fig. 15** Stress biaxiality at the surface for $t/R_1$=0.4 and ν=0.25 (blue $\sigma_2/\sigma_1$=0, green=0.5, red=1).

#### 4.1.2 Influence of the contact area of loading forces

Figure 16 gives the stresses for varying Hertzian contact areas. The Hertzian contact radius was chosen to be $a$=0 (point forces), $a$=0.01$R_1$, and $a$=0.003$R_1$. Only in regions very close to the contact centres can slight differences in stresses be found (see Fig. 16b). Due to the reduced importance of point loads in the 3-balls-on-3-balls test, the small effects near the contact areas may be neglected. All remaining results were obtained for a Hertzian contact radius of $a$=0.003 $R_1$.

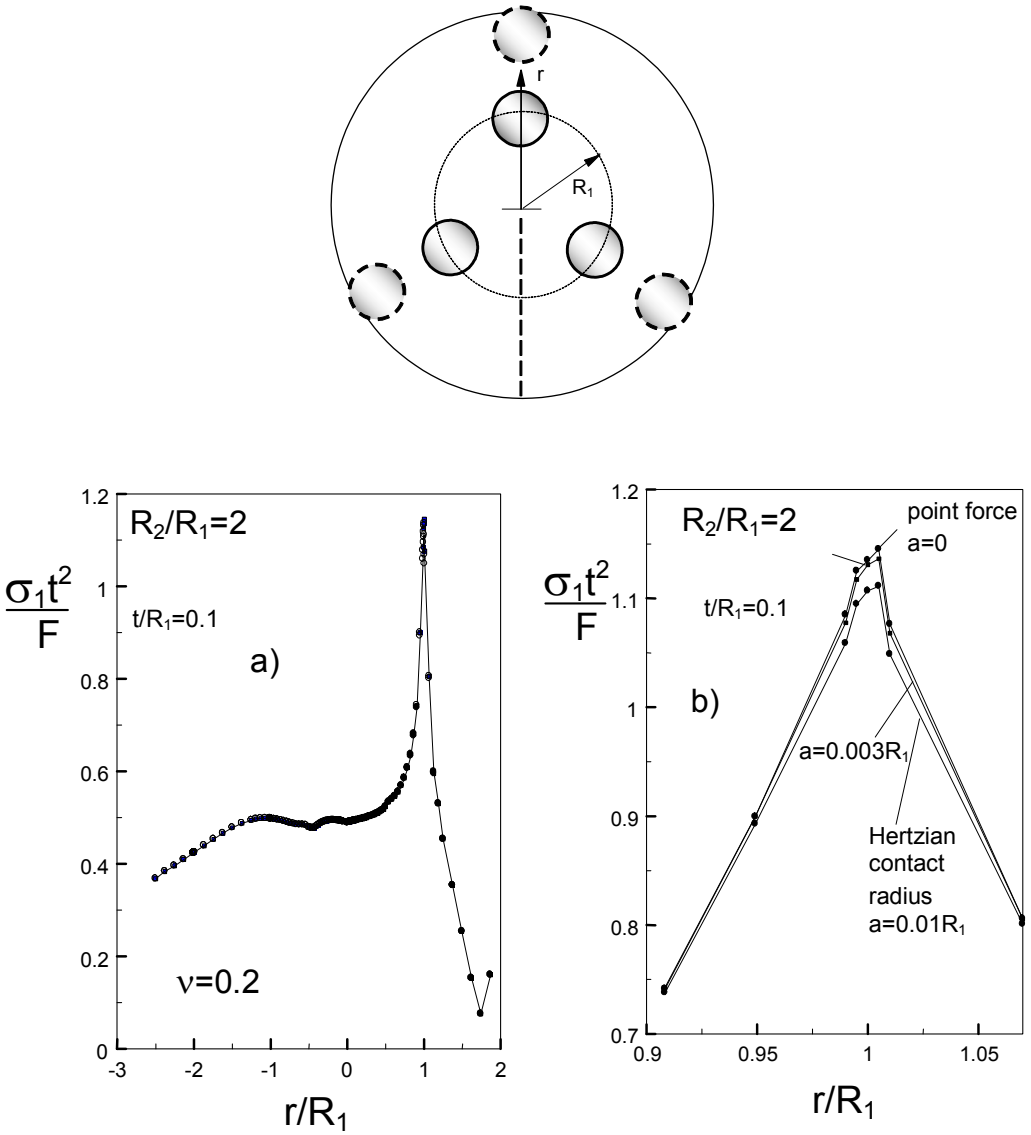


**Fig. 16** Influence of the load application area on maximum principal stress.

#### 4.1.3 Influence of disk thickness

The influence of disk thickness $t$ on the stresses is shown in Fig. 17. General proportionality $\sigma \propto 1/t^2$ can be concluded from the coincidence of the normalised stresses in the form of $\sigma t^2/F$ at larger distance from the contact zones.

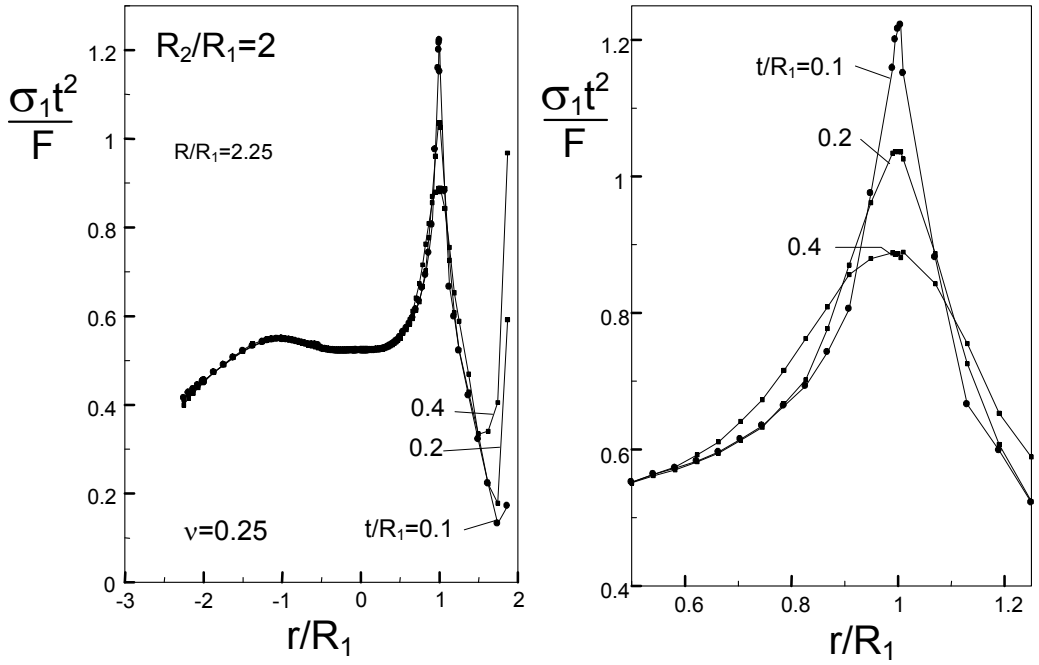


**Fig. 17** Maximum principal stress: Influence of specimen thickness.

#### 4.1.4 Influence of Poisson's ratio

Figures 18-20 show the effect of Poisson's ratio ν. The maximum principal stress increases slightly with increasing ν.

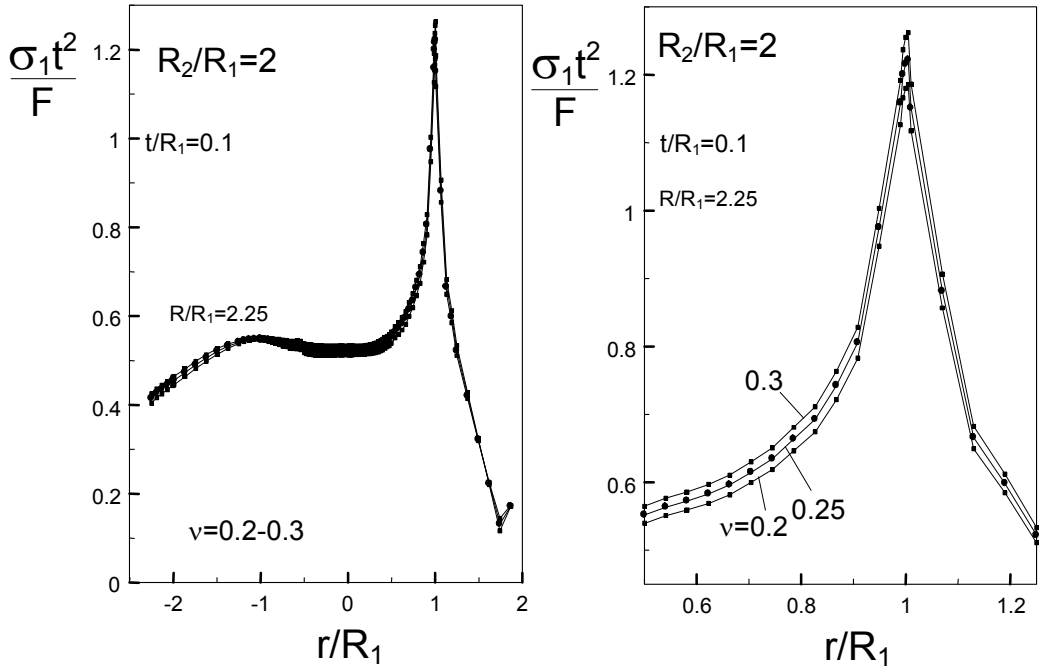


**Fig. 18** Influence of Poisson's ratio on the maximum principal stress for $t/R_1$=0.1.

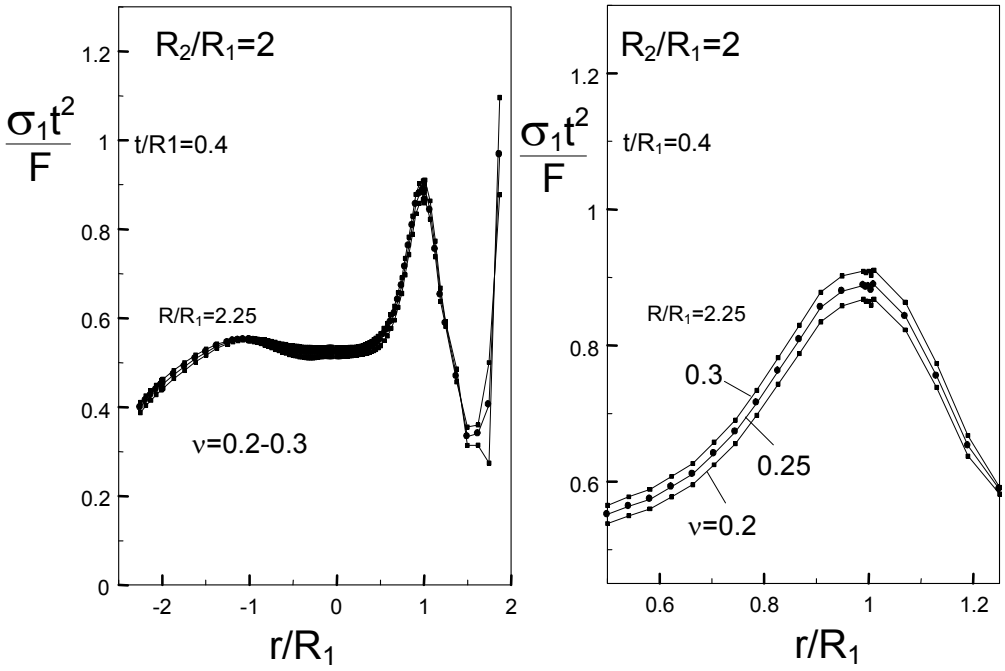


**Fig. 19** Influence of Poisson's ratio on the maximum principal stress for $t/R_1$=0.4.

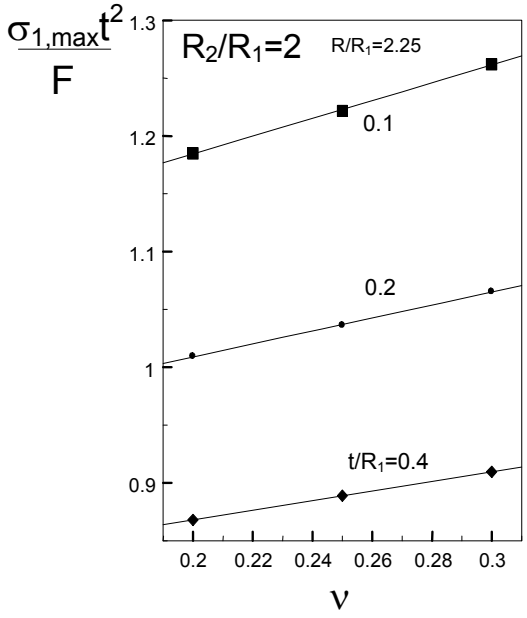


**Fig. 20** Maximum values of the maximum principal stress as a function of Poisson's ratio ν.

For a disk with $R/r_1$=2.25 under "sphere-in-line" conditions, the FE results can be expressed by

$$\sigma_{1,\max}\frac{t^2}{F} = 0.656\left(\frac{t}{R_1}\right)^{-0.196} + 0.274\left(\frac{t}{R_1}\right)^{-0.448}\nu \qquad (1)$$

### 4.1.5 Influence of disk diameter and overhang

The disk radius $R$ was varied within $2.25 \le R/R_1 \le 3$ defining the overhang. The influence of this parameter is visible from Figs. 21 and 22. Figure 22 and Table 4.1 list all results obtained for the maximum principal stress.

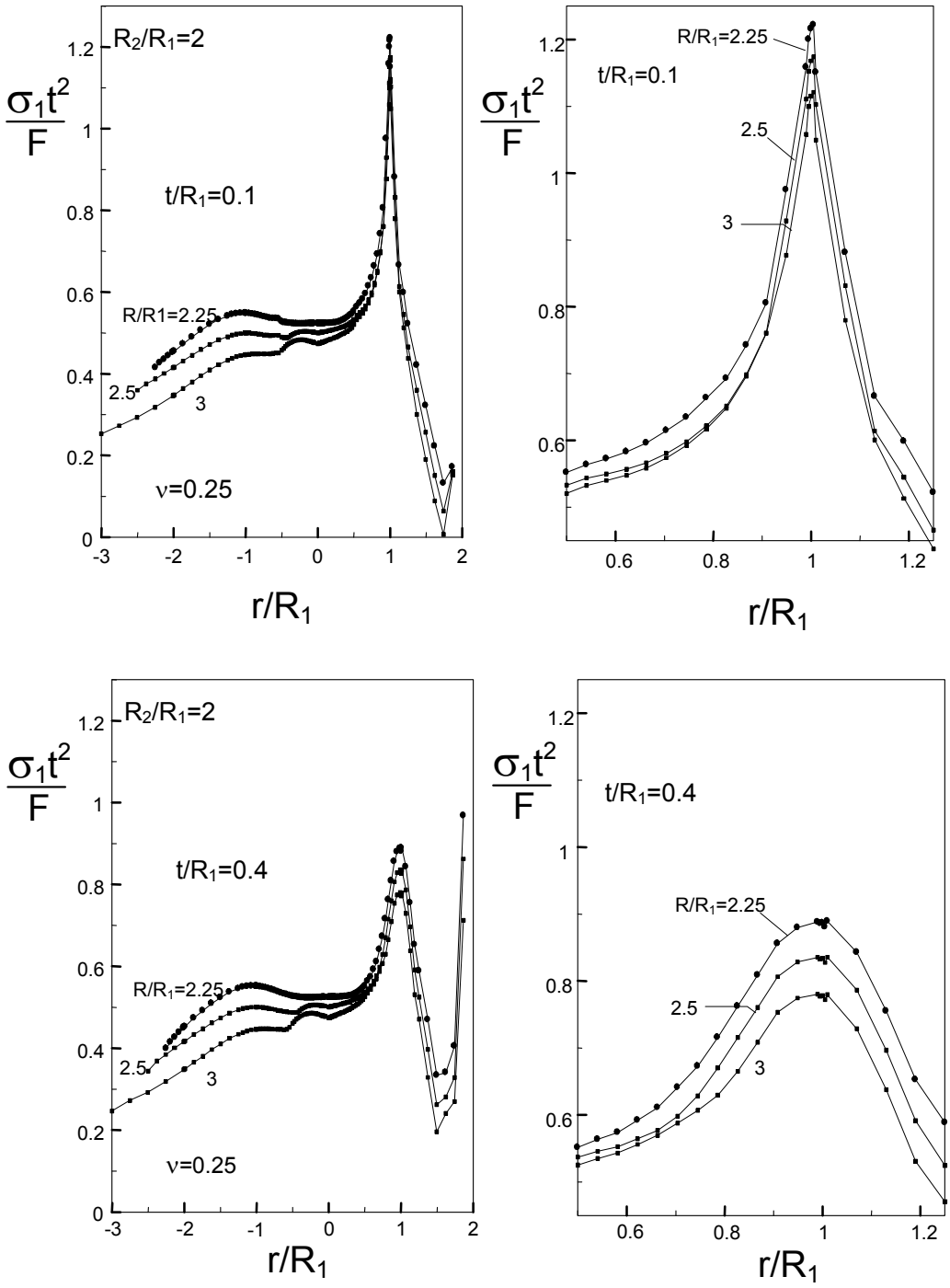


**Fig. 21** Influence of the overhang on maximum principal stress.

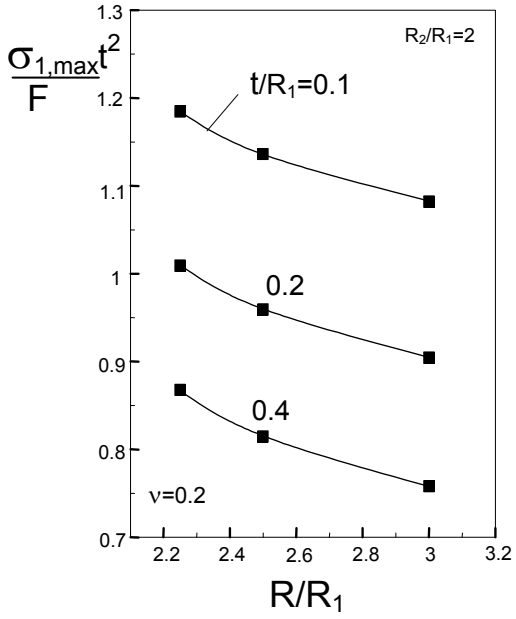


**Fig. 22** Maximum values of the maximum principal stress as a function of the plate thickness $t$ and Poisson's ratio ν.

| $t/R_1$ | $R/R_1$ | ν=0.2 | ν=0.25 | ν=0.3 |
|---|---|---|---|---|
| 0.1 | 2.25 | 1.185 | 1.222 | 1.262 |
| | 2.5 | 1.137 | 1.174 | 1.215 |
| | 3 | 1.082 | 1.121 | 1.164 |
| 0.2 | 2.25 | 1.009 | 1.036 | 1.065 |
| | 2.5 | 0.959 | 0.987 | 1.017 |
| | 3 | 0.905 | 0.934 | 0.965 |
| 0.4 | 2.25 | 0.868 | 0.889 | 0.909 |
| | 2.5 | 0.815 | 0.836 | 0.857 |
| | 3 | 0.758 | 0.780 | 0.803 |

**Table 4.1** Maximum values of $\sigma_1 t^2/F$.

### 4.2 Stresses for a ball-on-3-balls arrangement

The stress state of the ball-on-3-balls test was studied extensively by Börger et al.[23]. Some own results are given in Figs. 23 and 24 for a comparison of stresses and stress ratios with the results of a 3-balls-on-3-balls test.

From Fig. 23a, it can be concluded that the stresses in the 3-balls-on-3-balls test are significantly reduced compared to those occurring in the ball-on-3-balls test. The reason is that in the 3-balls-on-3-balls test total load is divided up into 3 partial loads.

More homogeneous stress distributions and biaxiality ratios are obvious (cf. e.g. Fig. 24b with Fig. 15).

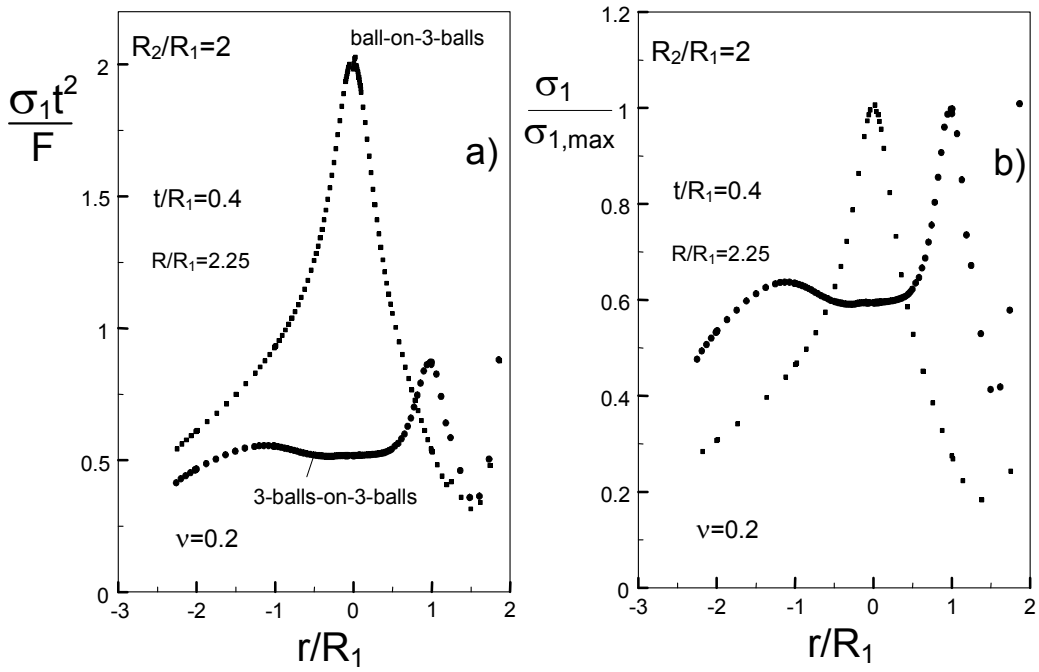


**Fig. 23** a) Maximum principal stress in a ball-on-3-balls test compared with the results of a 3-balls-on-3-balls test (balls in line), b) normalised representation.

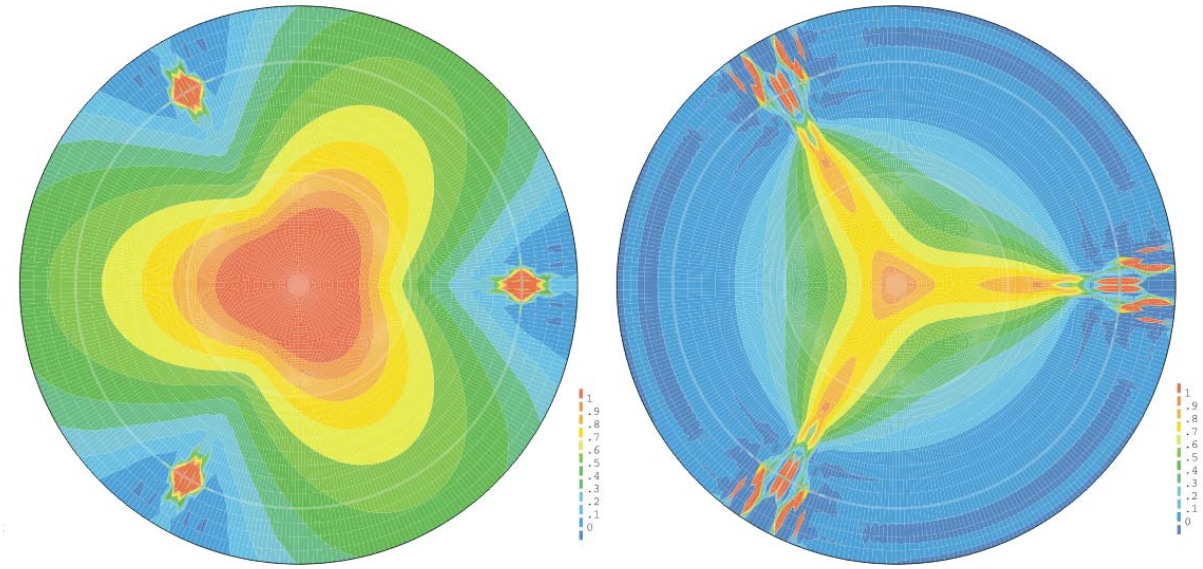

**Fig. 24** Contour plots of the stresses in a ball-on-3-balls test; left: Maximum principal stress (blue $\sigma_1 t^2/F$=0, green =0.5, red=1), right: Biaxiality ratio (blue $\sigma_2/\sigma_1$=0, green=0.5, red=1).

### 4.3 Loading and supporting balls under an angle of 60°

Figures 25-30 represent the stresses in the case of the inner balls being rotated by 60°.

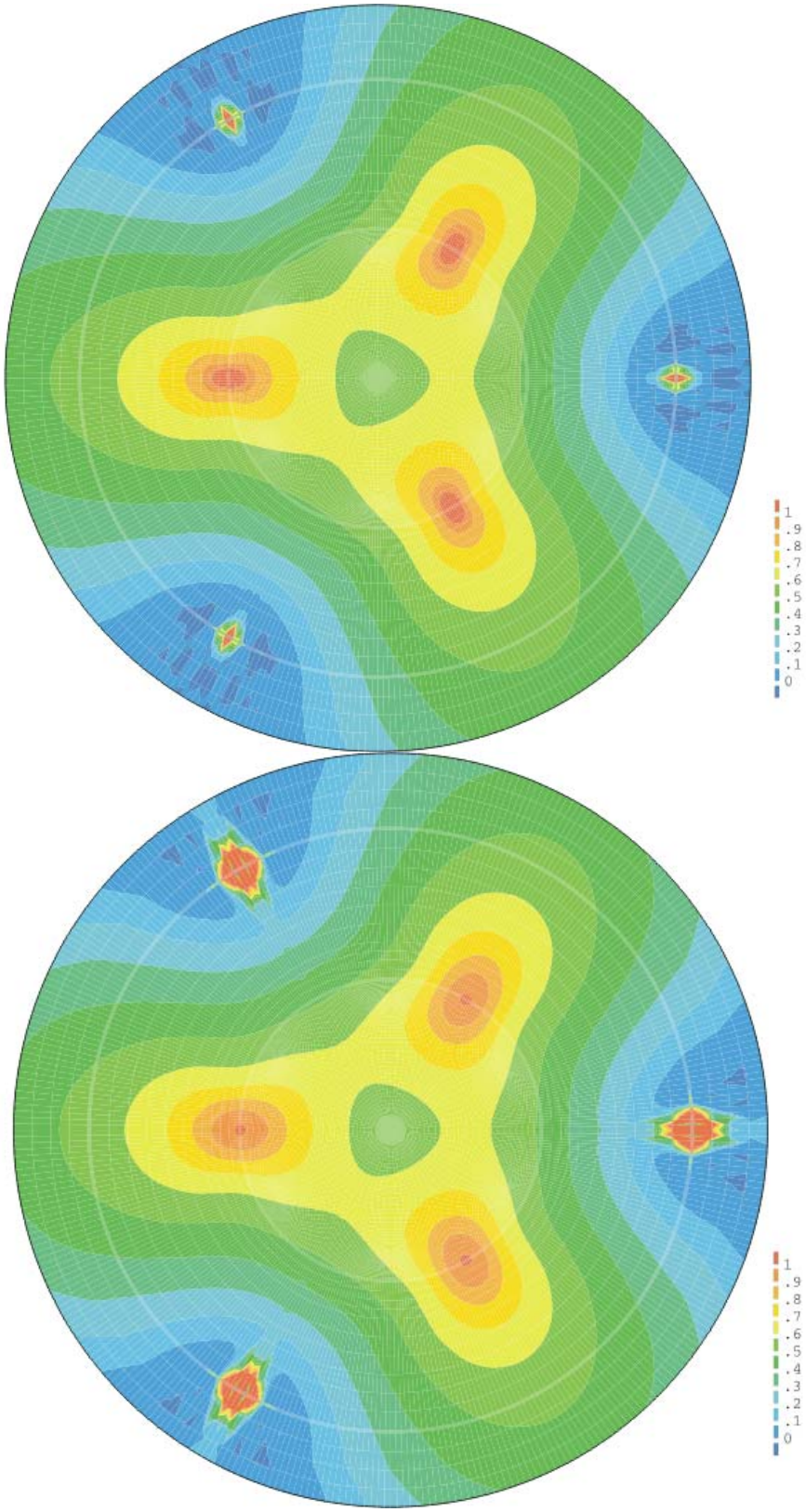


**Fig. 25** Maximum principal stress for a disk of $t/R_1$=0.1 (upper contour plot) and $t/R_1$=0.4 (lower plot) at ν=0.25 (blue $\sigma_1 t^2/F$=0, green =0.5, red=1).

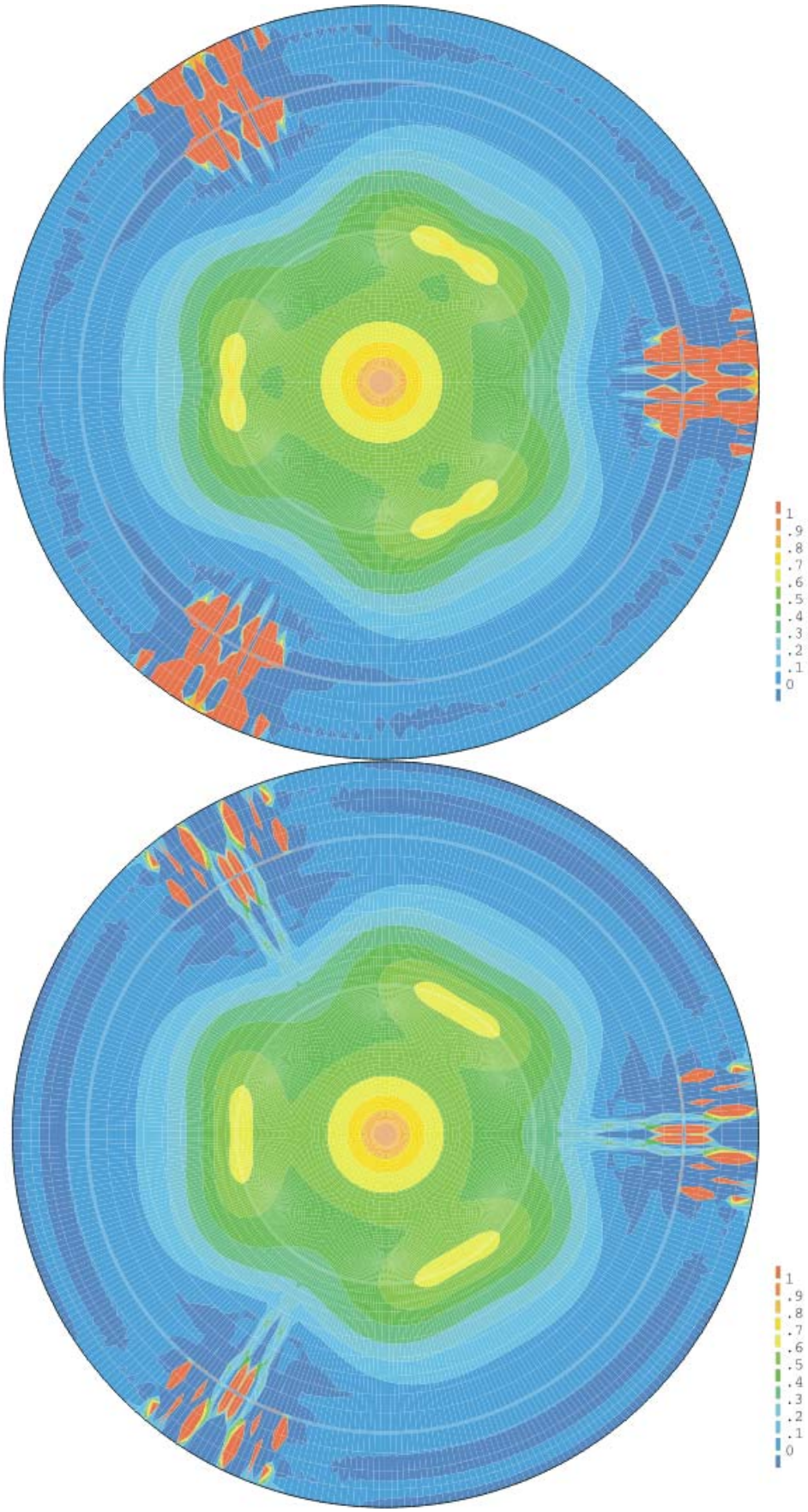


**Fig. 26** Stress biaxiality at the surface for a disk with $t/R_1$=0.1 (upper contour plot) and $t/R_1$=0.4 (lower plot) at $\nu$=0.25 (blue $\sigma_2/\sigma_1$=0, green=0.5, red=1).

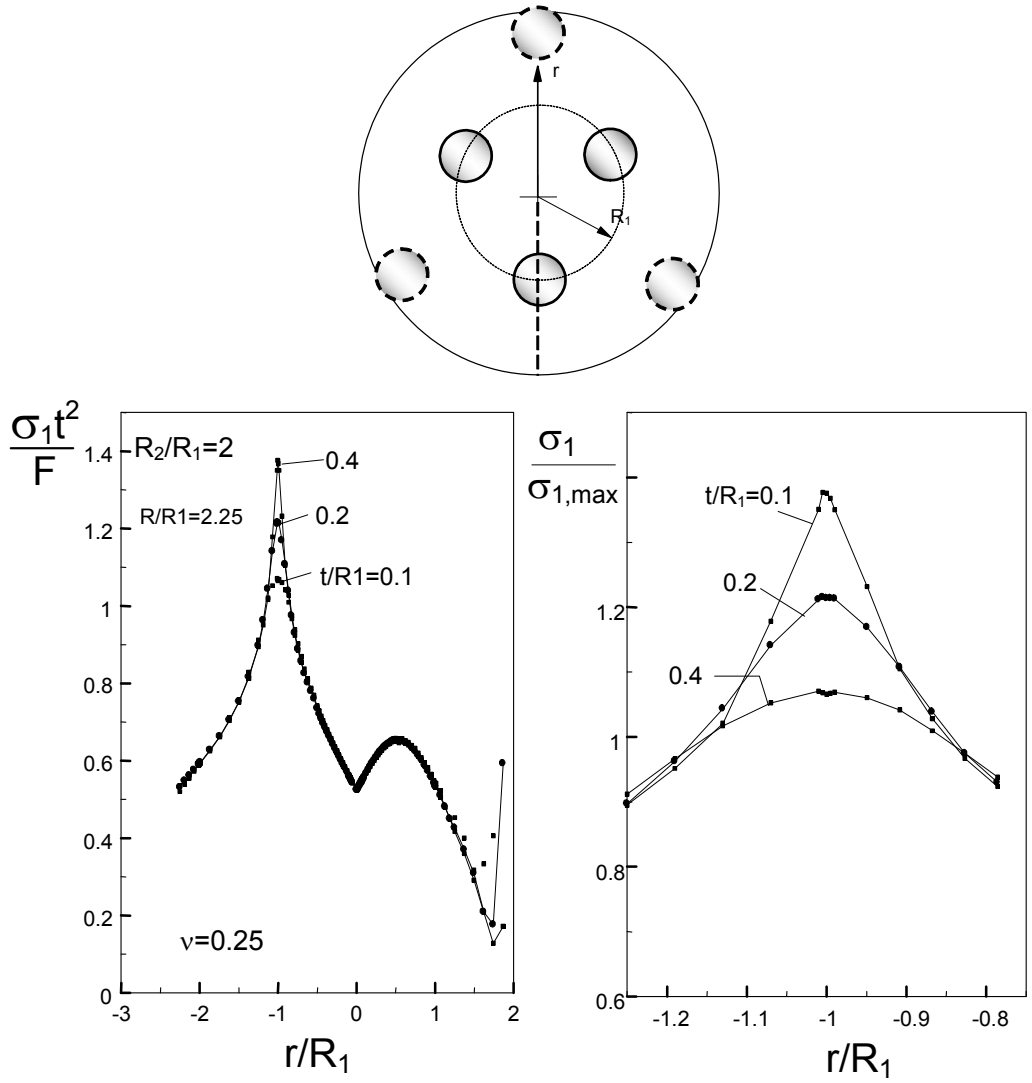


**Fig. 27** Maximum principal stress: Influence of specimen thickness (rt $r$=0, an equibiaxial stress state occurs. Here, the stress component that defines the maximum principal stress changes).

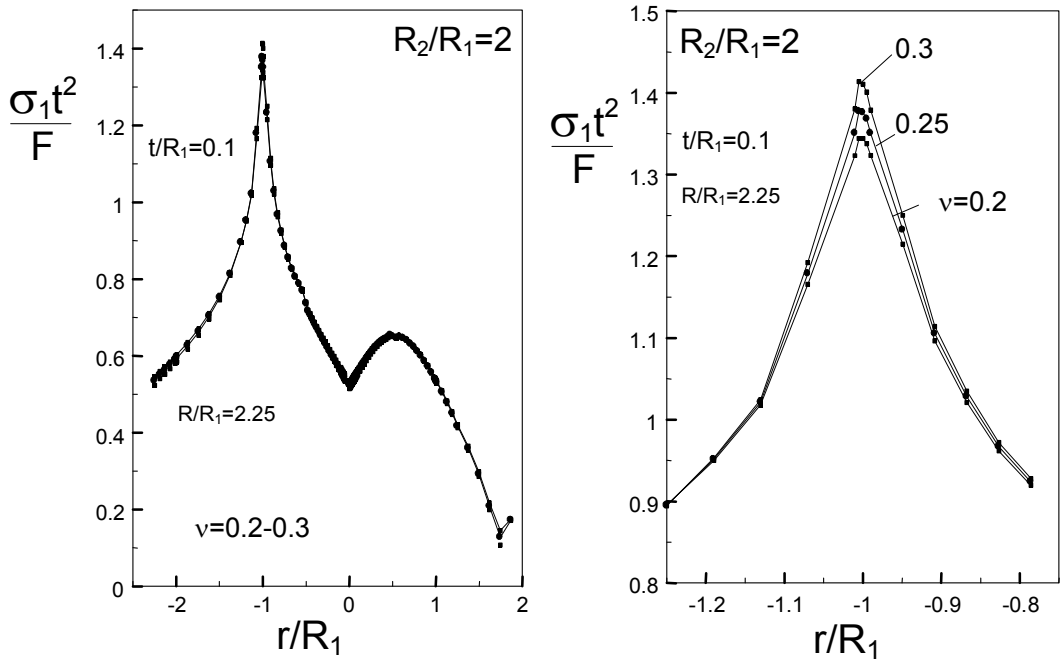

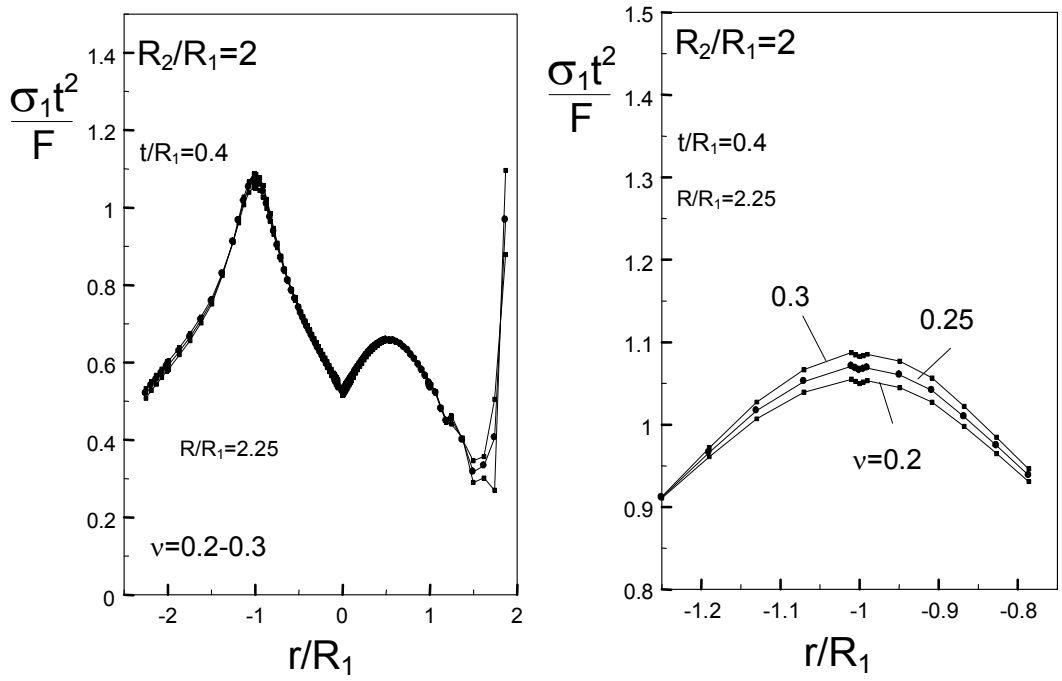


**Fig. 28** Maximum principal stress: Influence of Poisson's ratio.

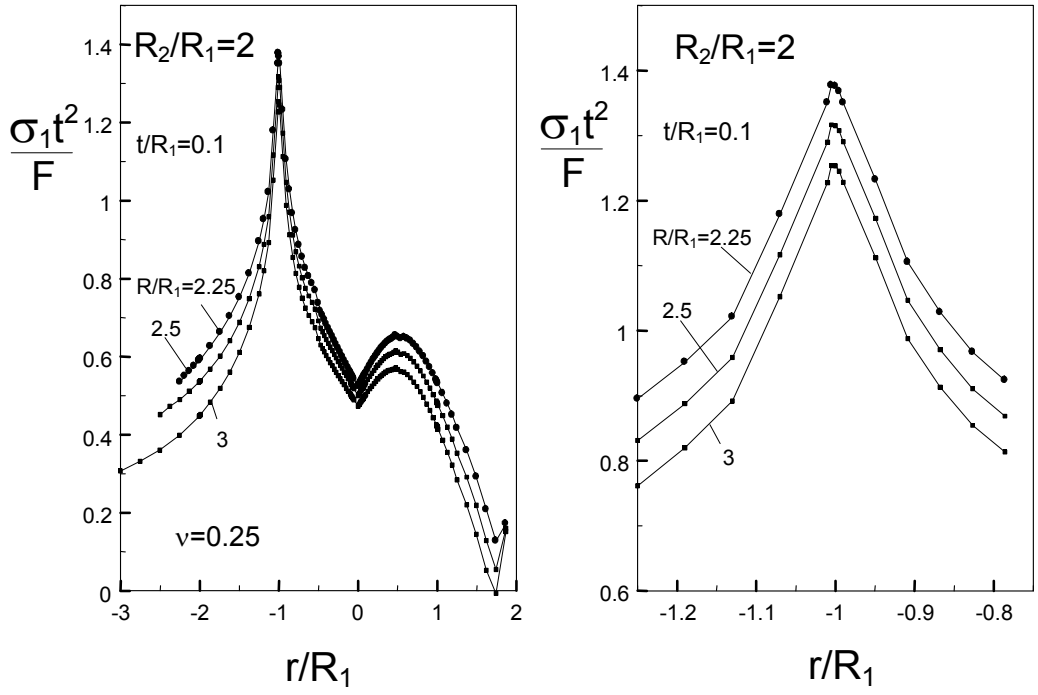

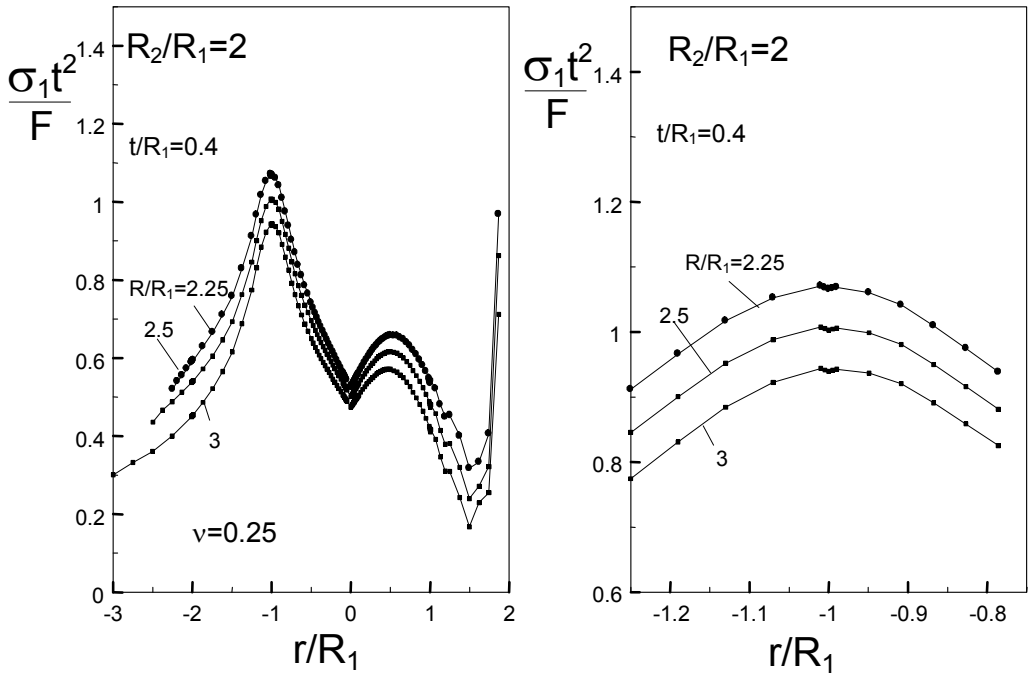


**Fig. 29** Maximum principal stress: Influence of the overhang.

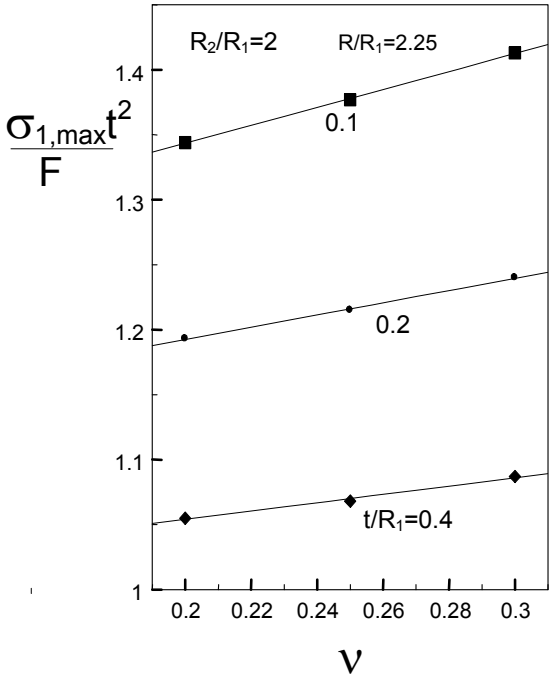


**Fig. 30** Maximum values of the maximum principal stress as a function of Poisson's ratio ν.

| $t/R_1$ | $R/R_1$ | ν=0.2 | ν=0.25 | ν=0.3 |
|---|---|---|---|---|
| 0.1 | 2.25 | 1.344 | 1.377 | 1.413 |
| | 2.5 | 1.283 | 1.316 | 1.353 |
| | 3 | 1.219 | 1.254 | 1.293 |
| 0.2 | 2.25 | 1.193 | 1.215 | 1.240 |
| | 2.5 | 1.131 | 1.154 | 1.178 |
| | 3 | 1.067 | 1.091 | 1.118 |
| 0.4 | 2.25 | 1.055 | 1.068 | 1.087 |
| | 2.5 | 0.991 | 1.007 | 1.025 |
| | 3 | 0.925 | 0.943 | 0.962 |

**Table 4.2** Maximum values of $\sigma_1 t^2/F$.

For $R/R_1$=2.25 and $0.1 \le t/R_1 \le 0.4$, the maximum stress values can be approximated by

$$\sigma_{1,\max}\frac{t^2}{F} = 0.871\left(\frac{t}{R_1}\right)^{-0.142} + 0.197\left(\frac{t}{R_1}\right)^{-0.533}\nu \tag{2}$$

## References


[1] Munz, D., Fett, T., CERAMICS: Mechanical Properties, Failure Behaviour, Materials Selection, Springer, Berlin, 1999.

[2] Maier, H.R., Heckel, K., Bruchwahrscheinlichkeit von polykristallinem Aluminium-oxid unter statischer Biege- und Zugbeanspruchung bei 800°C, Ber. Deutsche Keram. Ges. **54**(1977), 370-373.

[3] Giovan, M.N., Sines, G., Strength of a ceramic at high temperatures under biaxial and uniaxial tension, J. Amer. Ceram. Soc. **64**(1981), 68-73.

[4] Sines, G., Adams, M., Compression testing of ceramics, Fracture Mechanics of Ceramics, Vol.3, Plenum Press, New York, (1978), 403-434.

[5] Rice, R.W., The compressive strength of ceramics, in: Ceramics in several Environments, Vol.5, Plenum Press, New York, (1970), 195-229.

[6] Lankford, J., Davidson, D.L., The effect of compressive strength on the mechanical performance of strong ceramics, ICM 3, Vol.3, Cambridge, 1979, 35-43.

[7] ASTM C1161, Flexural strength of advanced ceramics at ambient temperatures.

[8] German Standard DIN 50110 Prüfung von Gusseisen, Biegeversuch, 1962-02.

[9] ENV 843/1 Advanced technical ceramics - mechanical properties of monolithic ceramics at room temperature - Part 1: flexural strength tests.

[10] German Standard DIN 1230, Steinzeug für die Kanalisation: Sonderformstücke und Übergangsbauteile.

[11] de With, G., Note on the use of the diametral compression test for the strength measurement of ceramics, J. Mater. Sci. Letters **3**(1984), 1000-1002.

[12] Evans, J.R.G., Stevens, R., The C-ring test for the strength of brittle materials, Brit. Ceram. Trans. Journ. **83**(1984), 14-18.

[13] Timoshenko, S., Young, D.H., Elements of Strength of Materials, van Nostrand (1968).

[14] Giovan, M.N., Sines, G., Strength of a ceramic at high temperatures under biaxial and uniaxial tension, J. Amer. Ceram. Soc. **64**(1981), 68-73.

[15] German Standard DIN 52292, Teil 1: Prüfung von Glas und Glaskeramik, Bestimmung der Biegefestigkeit, Doppelring-Biegeversuch an plattenförmigen Proben mit kleinen Prüfflächen, Teil 2: Prüfung von Glas und Glaskeramik, Bestimmung der Biegefestigkeit, Doppelring-Biegeversuch an plattenförmigen Proben mit großen Prüfflächen.

[16] Schmitt, W., Blank, K., Schönbrunn, G. (1983): Experimentelle Spannungsanalyse zum Doppelringversuch, Sprechsaal **116**, 397-405.

[17] Fessler, H., Fricker, D.C. (1984): A theoretical analysis of the ring-on-ring loading disc test, J. Amer. Ceram. Soc. **67**, 582-588.

[18] Soltész, U., Richter, H., Kienzler, R. (1987): The concentric ring test and its application for determining the surface strength of ceramics, in High Tech Ceramics, Elsevier Science Publishers, 149-158.

[19] Shetty, K.D., Rosenfield, A.R., McGuire, P., Duckworth, W.H. (1980): Biaxial flexure test for ceramics, Amer. Ceram. Soc. Bulletin **59**, 1193-1197.

[20] Shetty, K.D., Rosenfield, A.R., McGuire, Bansal, G.K., Duckworth, W.H. (1981): Biaxial fracture studies of a glass ceramic, J. Amer. Ceram. Soc. **64**, 1-4.

[21] de With, G., Wagemans, H.H.M., Ball-on-ring test revisited, J. Amer. Ceram. Soc. **72**(1989), 1538-1541.

[22] Godfrey, D. J. and John, S., Disc flexure tests for the evaluation of ceramic strength, In *Proceedings 2nd International Conference of Ceramic Materials and Components for Engines*. Verlag Deutsche Keramische Gesellschaft, Lübeck-Travemünde, 14–17 April 1986, pp. 657–665.

[23] Börger, A., Supancic, P., Danzer, R., The ball on three balls test for strength testing of brittle discs: stress distribution in the disc, J. Europ. Ceram. Soc. **22**(2002), 1425-1436.
[24] Börger, A., Supancic, P., Danzer, R., The ball on three balls test for strength testing of brittle discs: Part II: analysis of possible errors in the strength determination, J. Europ. Ceram. Soc. 24(2004), 2917-2928.
[25] Carneiro, F.L.L.B., Barcellos, A., Résistance à la traction des bétons, Instituto Nacional de Technologia, Rio de Janeiro (1949).
[26] Wright, P.J.F., Comments on an indirect tensile test on concrete cylinders, Magazine of Concrete Research **7**(1955), 87-96.
[27] Shaw, M.C., Braiden, P.M., De Salvo, G.J., The disk test for brittle materials, Trans. ASME, J. of Basic Engng. and Industry, (1975) 77-87.
[28] Hondros, G., The evaluation of Poisson's ratio and the modulus of materials of a low tensile resistance by the Brazilian (indirect tensile) test with particular reference to concrete, Australian J. Appl. Sci. **10**(1959), 243-268.
[29] Marion, R. H., Johnstone, J.K., A parametric study of the diametral compression test for ceramics, Am. Ceram. Soc. Bull. **56** (1977), 998-1002.
[30] Spriggs, R.M., Brissette, L.A., Vasilos, T., Tensile strength of polycrystalline ceramics by the diametral compression test, J. Mater. Res. Stand. **4**(1964).
[31] Szendi-Horvath, G., Fracture toughness determination of brittle materials using small to extremely small specimens, Engng. Fract. Mech. **13**(1980), 955-961.
[32] Petroski, H.J., Ojdrovic, R.P., The concrete cylinder: Stress analysis and failure modes, Int. J. Fract. **53**(1987), 263-279.
[33] Brückner-Foit, A., Fett, T., Munz, D., Schirmer, K., Discrimination of multiaxiality criteria with the Brazilian disc test, J. Europ. Ceram. Soc. **17**(1997), 689-696.
[34] Hasselman, D.P.H., Figures-of-merit for the thermal stress resistance of high-temperature brittle materials: a review, Ceramurgia Int. **4**(1978), 147.
[35] Swain, M.V., R-curve behaviour and thermal shock resistance of ceramics, J. Am. Ceram. Soc. **73**(1990), 621-628.
[36] Sato, S., Awaji, H., Kawamata, K., Kurumada, A., Oku, T., Fracture criteria of reactor graphite under multiaxial stresses, Nuclear Engng. and Design **103**(1987), 291-300.
[37] Ely, R.E., Strength of titania and aluminum silicate under combined stresses, J. Amer. Ceram. Soc. **55**(1972), 347-350.
[38] Adams, M., Sines, G., Determination of biaxial compressive strength of a sintered alumina ceramic, J. Amer. Ceram. Soc. **59**(1976), 300-304.
[39] Boutman, L.J., Krishnakuman, S.M., Mallick, P.K., Effects of combined stresses on fracture of alumina and graphite, J. Amer. Ceram. Soc. **53**(1970), 649-654.
[40] Fett, T., Oberacker, R., Vorrichtung zur Bestimmung der Festigkeit von keramischen Scheibenproben, Patentanmeldung 2004.